Structural Properties of $PbTiO_3$ and $PbZr_xTi_{1-x}O_3$: a Quantum-Chemical Study

ARVIDS STASHANS,[a, b] CESAR ZAMBRANO,[b, a] ALFREDO SANCHEZ,[b, a] LUIS MIGUEL PROCEL [b, a]

[a] *Centro de Investigación en Física de la Materia Condensada, Corporación de Física Fundamental y Aplicada, Apartado 17-12-637, Quito, Ecuador*

[b] *Departamento de Química, Colegio Politécnico, Universidad San Francisco de Quito, Apartado 17-12-841, Quito, Ecuador*

ABSTRACT: We investigate the structural and electronic properties of a pure and Zr-doped $PbTiO_3$ crystals. Nature of atomic relaxation around the Zr impurity is studied through quantum-chemical simulations based on the Hartree-Fock theory and a periodic large unit cell (LUC) model adopted within the so-called intermediate neglect of differential overlap (INDO) approximation. The most stable defect configurations are predicted for different impurity concentrations. The obtained results are compared with another theoretical studies and a number of experimental measurements carried out on this technologically important perovskite-type crystal.

Key words: $PbTiO_3$; $PbZrTiO_3$; LUC; impurity-doping; structural and electronic properties

Introduction

Ferroelectric materials are now the focus of intense study because of their unusual properties and a wide range of applications. Lead titanate ($PbTiO_3$) is one of the perovskite-type titanates having a chemical formula $ATiO_3$ where A is one of the following cations: Ba, Sr, Ca or Pb. The perfect perovskite structure is very simple and has a cubic symmetry. Its lattice consists of corner sharing oxygen octahedra with interpenetrating simple cubic lattices of A and Ti cations. The Ti cations sit at the center of each oxygen octahedra while the A metal ions lie in 12-fold coordinated sites between the octahedra. At 766 K lead titanate switches to tetragonal phase and becomes ferroelectric. Therefore, in order to understand more completely different properties of this material both phases need to be studied.

Ferroelectric materials such as $PbTiO_3$ are characterized by a nonvolatile, reversible polarization field that has been successfully used in radiation hard memories [1]. Lead titanate doped with Zr impurities, $PbZr_xTi_{1-x}O_3$, so-called PZT ceramics are ferroelectric oxides whose piezoelectric, dielectric and ferroelectric properties make them attractive for many applications. PZT ceramics have been proposed as high density storage media and integrated components for applications in dynamic and nonvolatile random access memories, as well as in surface acoustic wave devices, micromechanical devices and ferroelectric field effect devices [2-4]. These materials also promise dramatic improvements in the resolution and range of ultrasonic and sonar listening devices [5].

In spite of the fact that titanates have been subject of investigations since the discovery of ferroelectricity in barium titanate in the 1940s [6], there is still no complete

understanding of a main part of their properties at the fundamental level. Numerous applications and unresolved fundamental scientific questions have attracted considerable attention from the scientific community. The electronic structure of lead titanate has been studied extensively using different theoretical methods [7-9]. It also has been discovered that the covalent interaction between Ti and O ions is important for the occurrence of ferroelectricity in the $PbTiO_3$ crystal [10, 11].

Regarding doping with zirconium, it is relevant to mention that PZT is a newly discovered relaxor-PT material having high-electromechanical coupling properties and low-dielectric loss. Nevertheless, it has not been sufficiently studied at the fundamental (quantum-chemical) level. A lot of experimental measurements have been collected applying various techniques. Few recent examples include atomic force microscopy measurements of control and imaging of ferroelectric domains over large areas with nanometer resolution [12], high resolution X-ray diffraction experiments to study the origin of the piezoelectric response [13], a highly reproducible resistance modulation experiments [14] and synchrotron X-ray powder diffraction measurements of the morphotropic phase boundary in this material [15].

The objective of our work is to study the equilibrium geometry of a Zr impurity in the $PbTiO_3$ cubic and tetragonal lattices as well as the lattice distortion due to the impurity doping and compare our results with the available experimental and theoretical findings. We also provide a new parametrization scheme for the $PbTiO_3$ crystal in order to study its electronic and structural properties. The discussion is done in a comparative manner for the cubic lattice *versus* the tetragonal one. The article is organized as follows: In the second section, the parametrization scheme for the $PbTiO_3$ crystal is given and a short description of the periodic large unit cell (LUC) model is outlined.

The third section deals with computations of the perfect crystal properties. The fourth and fifth sections provide results on the doping of one and two Zr impurities in both crystallographic lattices and their effects upon the structural properties of the material. In the sixth section, important conclusions are outlined.

Periodic LUC Model and $PbTiO_3$ Parametrization

A periodic large unit cell (LUC) model [16] is used, which is implemented into the SYM-SYM computer code [17]. The calculations are carried out using a (nonrelativistic) valence basis set of lead 6s, 6p, and 5d atomic orbitals (AOs), titanium 3d, 4s, and 4p AOs and oxygen 2s and 2p AOs. The main computational equations for calculating the total energy of the crystal within the framework of the LUC model are described elsewhere [16, 18]. Here we point out that the basic idea of the LUC formalism is referred to the so-called $\boldsymbol{k} = 0$ approximation. In this case the Fock matrix elements are made self-consistent through

$$\frac{1}{N}\sum_{k} P_{pq}(\vec{k})\exp(i\vec{k}\cdot\vec{R}_v) \qquad (1)$$

where the summation is carried out over all $\boldsymbol{k}$ values in the reduced Brillouin zone (BZ) of the LUC. Thus, the information obtained corresponds only to the point $\boldsymbol{k} = 0$ of the density matrix $P_{pq}(\boldsymbol{k})$. However, this is equivalent to a band structure calculation at those $\boldsymbol{k}$ points, which transform to the BZ center on extending the primitive unit cell. In this work, a 40-atom LUC was used, which corresponds to an eight-fold (2x2x2) extended primitive unit cell. This means that eight $\boldsymbol{k}$ points were included in our band structure calculations. As it was shown in many recent studies [19-21], an eight-fold or even four-

fold-symmetric extension of the primitive unit cell proves to be sufficient to reproduce almost exactly the electronic band structure of a given crystal. It is also important to mention that the periodic LUC model is free from the limitations of different cluster models applicable mainly to materials with a wide band gap. Using the LUC model one can precisely calculate impurity concentrations. This consideration was very important in our studies.

The quantum-chemical method implemented into the SYM-SYM computer code is based on the Hartree-Fock (HF) theory and additionally contains a number of adjustable parameters. These numerical parameters simplify specific two-center integrals in the semi-empirical INDO approximation and make it applicable to study complex systems usually not suitable for non-empirical methods. The former method is not cumbersome and time consuming in the treatment of electronic and spatial structure of systems, especially with partially covalent chemical bonding like oxide crystals. In particular, the computer code has the important advantage of geometry prediction for crystals doped with impurity atoms [22, 23]. It is relevant to state that with this method no-*a priori* assumption is made upon the pattern of the electronic density distribution in the vicinity of the defect under study, i.e.: it is obtained using a self-consistent-field (SCF) approach. This produces reliable information about the defect influence upon the electronic band structure properties. Since the numerical parameters can partially take into account electron correlation effects, the electronic band structure can often be reproduced even more precisely than the corresponding *ab initio* techniques. For instance, the band-gap width for the TiO_2 crystal [24] was obtained closer to the experimental value compared to the corresponding value calculated by an *ab initio* HF method [25].

Relativistic effects for the Pb atom were indirectly taken into account by reproducing the $PbTiO_3$ crystal band structure properties. This was accomplished in the same manner as previously published for the W atom [26], by manipulating the atomic parameters and by incorporating into our computer code special pseudo-potentials [27]. The important feature of these potentials is that relativistic effects are included in a way that enables the pseudopotentials to be used in nonrelativistic formulations. The optimization of numerical parameters within the INDO method for a given chemical element includes the reproduction of the following data: the main features of the electronic structure (width of the forbidden energy gap, widths of the valence bands, density of states [DOS] of the energetic bands) and geometry (cubic and tetragonal lattice constants) of the crystal under study. The obtained Pb parameters are shown in Table I. The Ti parameters were also slightly modified to reproduce more precisely the band structure properties of the $PbTiO_3$ crystal. The O parameters were taken as standard [28]. Finally, we would like to note that in order to take into account the relativistic effects we had to refuse from the idea of generality and transferability of numerical parameters. That is why the parameters of Ti atom are different from those used in our previous works.

Our method has been shown to be very reliable in reproducing spatial and electronic properties of a wide variety of crystals, including oxide materials. For instance, the program code gave satisfactory results on defect studies in complex oxides such as α-Al_2O_3 [29-31], MgO [32], WO_3 [26] and TiO_2 [20-22, 33]. In the last five years the current method has been successfully used in studies of perfect and defective perovskite-type crystals. The examples include calculations of point defects and modeling of phase transition in $KNbO_3$ crystal [34, 35], Nb-doping in a $KTaO_3$ material

[36] and studies of pure and defective $BaTiO_3$ [37-39], $SrTiO_3$ [40, 41] and $CaTiO_3$ crystals [42].

Electronic Band Structure of a Pure $PbTiO_3$

A 4-atom LUC was used to calculate both cubic and tetragonal structures of lead titanate. The calculated DOS for the cubic phase, plotted in Figure 1, shows that the lower valence band is composed mainly of O 2s states with a small amount of Pb 5d states. The next filled energy band is exclusively Pb 5d in nature. This sub-band is very narrow which agrees well with other works [7]. Above the narrow Pb 5d band, the O 2p band was found which has some small admixture of Pb 5d states and Ti 3d AOs. The width of the O 2p valence band is overestimated due to the effect of the standard oxygen parameters [28], e.g.: the large values of the resonance integral parameter are equal to -16.0 eV and are responsible mainly for the width of the O 2p valence band. Finally, the upper valence band is composed of Pb 6s states having also a considerable contribution of O 2p states. The bottom of the conduction band is mainly Pb 6p in nature with a strong contribution of Ti 3d AOs. The calculated optical band gap using the ΔSCF method is found to be equal to 6.8 eV. The band gap value obtained as the difference between the highest occupied molecular orbital (HOMO) and lowest unoccupied molecular orbital (LUMO) is 7.3 eV. These values are considerably larger than the experimental value of 3.4 eV [43] due to the neglect of long-range correlation corrections. This is a common weakness of the methods based on the Hartree-Fock theory [44]. In general, our method reproduces with high precision the electronic band structure of cubic lead titanate and it is also in good agreement with studies carried out

by other groups [7-9, 45].

The calculated electronic band structure for the tetragonal phase shows a somewhat different pattern compared to the cubic phase of lead titanate. Although the widths of valence bands and their location is similar to the previous case, we find a large amount of Ti 3d states present in the O 2p valence band. This points to the hybridization between the Ti 3d and O 2p AOs, which accompanies the phase transition: cubic (paraelectric) $\rightarrow$ tetragonal (ferroelectric). This outcome implies the fact that the hybridization between the Ti 3d and O 2p is necessary for ferroelectricity in $PbTiO_3$ and it agrees very well with other reports in the literature [10]. Also due to hybridization effects, the charges on Ti atoms become more negative (see table II for more details). The calculated optical band gap is found to be equal to 4.8 eV as the difference between the HOMO and LUMO, and the value of 4.4 eV is obtained using the ΔSCF method. The reduction of the band gap testifies the presence of more covalent chemical bonding in the tetragonal phase of lead titanate compared to the cubic structure of this material.

It is worth mentioning that we managed to reproduce completely the lattice constants for both crystallographic lattices in accordance with the experimental data: a = 3.96 Å and a = 3.99 Å, c = 4.03 Å for the cubic and tetragonal lattices, respectively [46].

$PbZr_{0.125}Ti_{0.875}O_3$ Structural Properties

The same size LUC was used to study doping with Zr in $PbTiO_3$ lattices. In the case of a single impurity, one of the Ti atoms was substituted by Zr atom. Owing to the Zr insertion, which is a perturbation for the otherwise perfect crystalline lattice, one can

anticipate atomic displacements in order to reduce the total energy of the system. Different kinds of atomic relaxation were considered including non-symmetric lattice distortion and two spatial configurations, different for each one of the two crystallographic lattices, were obtained.

In the case of the cubic structure, it was found that the Zr-surrounding Pb atoms remained static while the six impurity-closest O atoms moved outwards by 0.19 Å each, (see Fig. 3) along the directions <100>. In the case of the tetragonal structure (see Fig. 4) outward movements for both O and Pb atoms were observed. Oxygens moved away from the Zr impurity along the <100> directions by 0.19 Å in the xy plane and by 0.20 Å along the z axis. The distinct relaxation along the z axis could be due to the ferroelectricity phenomenon, which is present in the tetragonal phase of this material. The eight Zr-nearest Pb atoms moved away from the impurity by 0.14 Å along the <111> directions. Thus, we can conclude that the atomic rearrangement due to the Zr-doping is symmetric in both structures but slightly larger O movements along the z axis were obtained for the tetragonal crystallographic lattice.

The observed oxygen outward movements for the cubic phase are expected because of the Coulomb interaction since the Zr atom is more negative (q_{Zr} = 2.08 ***e***) compared to the Ti atom (q_{Ti} = 2.55 ***e***) it has replaced. The same is true for the tetragonal phase, where we found q_{Zr} = 1.99 ***e*** and q_{Ti} = 2.47 ***e***. The outward movements of positively charged Pb atoms can be explained by the larger size of the Zr atom compared to the Ti atom, and a consecutive larger repulsion between overlapping electron clouds of the Zr impurity and its surrounding Pb atoms.

$PbZr_{0.25}Ti_{0.75}O_3$ Structural Properties

An impurity concentration x = 0.25 corresponds to Zr-doping when two of the eight Ti atoms are substituted by Zr atoms. There are different possibilities of how the Zr atoms can be found in the crystalline lattice. For the cubic structure there are three alternatives when the impurity atoms are situated in one of the following directions: <100>, <110> and <111>. In the tetragonal lattice, in addition to the above-mentioned arrangements there is one more alternative, a Zr located along <101>, which is different from one in the <110> direction.

Different kinds of atomic relaxations were considered for all above-mentioned possibilities; as a result, we obtained the following equilibrium defect configurations and corresponding lattice distortion. In the case of the cubic structure we found the same atomic displacements as in the case of a single impurity, i.e.: outward oxygen movements by 0.19 Å along the <100> direction (see Fig. 5). The equilibrium defect configuration having the lowest total energy was found for the Zr impurities situated along the <110> direction. Obviously, this impurity concentration gives the same perturbation by Zr atom within each of the two cubes and therefore this leads to the same host atom relaxation.

In the case of the tetragonal structure, the lowest energy configuration was found for the Zr atoms located along the <110> direction. For this configuration the atomic relaxation is as follows: The impurities-closest twelve O atoms move outwards along the directions <100> by 0.19 Å in the xy plane and by 0.16 Å along the z axis. The distinct relaxation along the z axis is again explained by the ferroelectricity effect. Additionally, the asymmetry in atomic displacements along the ferroelectric z axis was

also found in our previous impurity-doping studies in $SrTiO_3$ [40] and $BaTiO_3$ [38, 47] crystals.

Conclusions

The technologically important $PbTiO_3$ and $PbTiO_3$ (doped with Zr) were studied using a quantum-chemical method developed for crystals. The structural properties of pure lead titanate were reproduced very well demonstrating the reliability of our method. The analysis of the DOS shows considerable covalence effects in the chemical bonding for the tetragonal $PbTiO_3$ lattice. The observed hybridization between the Ti 3d and O 2p states points out the importance of this phenomenon regarding ferroelectricity in accordance with other studies [10].

The Zr-doping shows outward atomic movements with respect to the impurity atom. The lattice distortion can be partially explained by the Coulomb law and also by taking into account the fact that the impurity atom is larger than the Ti atom it substitutes.

ACKNOWLEDGMENTS

The authors thank Paul Sánchez for his help in the preparation of Figures 1 and 2. We are also grateful to Carlos Baraja for his assistance in designing Figures 3 to 5.

References

1. J. F. Scott and C. A. Paz de Araujo, Science **246**, 1400 (1989).
2. S. L. Swartz and V. E. Woods, Condens. Matter News **1**, 4 (1992).
3. G. H. Haertling, J. Vac. Sci. Technol. A **9**, 414 (1991).
4. C. H. Ahm, R. H. Hammond, T. H. Geballe, M. R. Beasley, J.-M. Triscone, M. Decroux, O. Fischer, L. Antognazza, and K. Char, Appl. Phys. Lett. **70**, 206 (1997).
5. R. F. Service, Science **275**, 1878 (1997).
6. A. von Hippel, Rev. Modern Phys. **22**, 221 (1950).
7. R. E. Cohen and H. Krakauer, Phys. Rev. B **42**, 6416 (1990).
8. K. M. Rabe and U. V. Waghmare, J. Phys. Chem. Solids **57**, 1397 (1996).
9. A. Garcia and D. Vanderbilt, Phys. Rev. B **54**, 3817 (1996).
10. R. E. Cohen, Nature **358**, 136 (1992).
11. K. Miura and M. Tanaka, Japan J. Appl. Phys. **37**, 6451 (1998).
12. T. Tybell, C. H. Ahn, and J.-M. Triscone, Appl. Phys. Lett. **72**, 1454 (1998).
13. R. Guo, I. E. Cross, S.-E. Park, B. Noheda, D. E. Cox, and G. Shirane, Phys. Rev. Lett. **84**, 5423 (2000).
14. Y. Watanabe, Phys. Rev. B **59**, 11257 (1999).
15. B. Nobeda, J. A. Gonzalo, I. E. Cross, R. Guo, S.-E. Park, D. E. Cox, and G. Shirane, Phys. Rev. B **61**, 8687 (2000).
16. A. L. Shluger and E. V. Stefanovich, Phys. Rev. B **42**, 9646 (1990).
17. L. Kantorovich and A. Livshicz, Phys. Status Solidi B **174**, 79 (1992).
18. R. A. Evarestov and V. A. Lovchikov, Phys. Status Solidi B **97**, 743 (1979).

19. A. Stashans and M. Kitamura, Solid State Commun. **99**, 583 (1996).

20. S. Lunell, A. Stashans, L. Ojamäe, H. Lindström, and A. Hagfeldt, J. Am. Chem. Soc. **119**, 7374 (1997).

21. P. Persson, A. Stashans, R. Bergström, and S. Lunell, Int. J. Quant. Chem. **70**, 1055 (1998).

22. A. Stashans, S. Lunell, R. Bergström, A. Hagfeldt, and S.-E. Lindquist, Phys. Rev. B **53**, 159 (1996).

23. A. Stashans and M. Kitamura, J. Phys. Chem. Solids **58**, 777 (1997).

24. A. Stashans, S. Lunell, and R. W. Grimes, J. Phys. Chem. Solids **57**, 1293 (1996).

25. A. Fahmi, C. Minot, B. Silvi, and M. Causà, Phys. Rev. B **47**, 11717 (1993).

26. A. Stashans and S. Lunell, Int. J. Quant. Chem. **63**, 729 (1997).

27. G. B. Bachelet, D. R. Hamann, and M. Schlüter, Phys. Rev. B **26**, 4199 (1982).

28. E. V. Stefanovich, E. K. Shidlovskaya, A. L. Shluger, and M. A. Zakharov, Phys. Status Solidi B **160**, 529 (1990).

29. A. Stashans, E. Kotomin, and J.-L. Calais, Phys. Rev. B **49**, 14854 (1994).

30. L. Kantorovich, A. Stashans, E. Kotomin, and P. W. M. Jacobs, Int. J. Quant. Chem. **52**, 1177 (1994).

31. E. A. Kotomin, A. Stashans, and P. W. M. Jacobs, Rad. Eff. Def. Solids **134**, 87 (1995).

32. R. I. Eglitis, M. M. Kuklja, E. A. Kotomin, A. Stashans, and A. I. Popov, Comput. Mater. Sci. **5**, 298 (1996).

33. L. Patthey, H. Rensmo, P. Persson, K. Westermark, L. Vayssieres, A. Stashans, Å. Petersson, P. A. Brühwiler, H. Siegbahn, S. Lunell, and N. Mårtensen, J. Chem. Phys. **110**, 5913 (1999).

34. R. I. Eglitis, A. V. Postnikov, and G. Borstel, Phys. Rev. B **54**, 2421 (1996).

35. E. A. Kotomin, R. I. Eglitis, A. V. Postnikov, G. Borstel, and N. E. Christensen, Phys. Rev. B **60**, 1 (1999).

36. R. I. Eglitis, E. A. Kotomin, and G. Borstel, J. Phys.: Condens. Matter **12**, L431 (2000).

37. A. Stashans and H. Pinto, Int. J. Quant. Chem. **79**, 358 (2000).

38. H. Pinto and A. Stashans, Comput. Mater. Sci. **17**, 73 (2000).

39. H. Pinto, A. Stashans, and P. Sánchez, *Defects and Surface-Induced Effects in Advanced Perovskites*, NATO Science Series, High Technology (Kluwer Academic Publishers, Dordrecht, 2000), Vol. 77, p. 67.

40. A. Stashans and P. Sánchez, Mater. Lett. **44**, 153 (2000).

41. A. Stashans, Mater. Chem. Phys. **68**, 124 (2001).

42. F. Erazo and A. Stashans, Phil. Mag. B **80**, 1499 (2000).

43. C. H. Peng, J. F. Chang, and S. B. Desu, Mat. Res. Soc. Symp. Proc. **243**, 21 (1992).

44. A. B. Kunz, Phys. Rev. B **6**, 606 (1972).

45. M. Kitamura and H. Chen, Ferroelectrics **210**, 13 (1998).

46. R. W. G. Wyckoff, *Crystal Structures* (Interscience, New York, 1960).

47. E. Patiño and A. Stashans, Ferroelectrics, in press (2001).

TABLE I (a)

Numerical parameter sets for Ca, Ti, O and La atoms.

Atom	AO	ζ (a.u.)	E_{neg} (eV)	-β (eV)	P^0 (*e*)
	6s	1.90	23.82	0.3	1.8
Pb	6p	1.85	16.8	0.3	0.2
	5d	2.90	36.8	29.0	2.00
	4s	1.75	1.5	0.8	0.44
Ti	4p	1.70	-2.0	0.8	0.22
	3d	1.88	0.07	8.0	0.55
O	2s	2.27	4.5	16.0	1.974
	2p	1.86	-12.6	16.0	1.96
	5s	1.90	8.0	0.5	1.0
Zr	5p	1.90	-8.0	0.5	0.0
	4d	1.83	4.6	11.0	0.6

TABLE I (b)

Two-center parameters $\alpha_{\mu B}$ (a.u.$^{-1}$), where $\mu \in$ A.

	B			
A	Pb	Ti	O	Zr
Pb	-0.04	-0.11	-0.22	-0.19
Ti	0.00	0.00	-0.03	-0.09
O	-0.18	-0.05	0.00	-0.15
Zr	0.00	0.00	-0.03	0.00

TABLE II

Charges on atoms for the perfect lead titanate (in *e*). Two different charges on oxygen for the tetragonal phase originates due to the two different crystallographic positions occupied by O atoms in this structure.

Atom	Cubic phase	Tetragonal phase
Pb	1.68	1.66
Ti	2.49	2.38
O	-1.39	-1.33 & -1.38

Figure Captions

FIGURE 1. Density of states (DOS) of the cubic phase of lead titanate. The four lowest energy bands (filled bands) correspond to O 2s, Pb 5d, O 2p and Pb 6s AOs, respectively. The bottom of the conduction band is composed of Pb 6p and Ti 3d states. The ‘zero’ value of the energy is attributed to the highest occupied molecular orbital.

FIGURE 2. DOS of the tetragonal phase of lead titanate. The four lowest energy bands (filled bands) correspond to O 2s, Pb 5d, O 2p and Pb 6s AOs, respectively.

FIGURE 3. Cubic lattice of lead titanate with Zr-surrounded O atoms moving outward. Small and large black balls represent oxygen and titanium atoms, respectively, while gray balls describe lead atoms.

FIGURE 4. Tetragonal lattice of lead titanate with Zr-surrounded six O atoms and eight Ti atoms moving outward. Small and large black balls represent oxygen and titanium atoms, respectively, while gray balls describe lead atoms.

FIGURE 5. Two-impurity doping in lead titanate structure with Zr atoms situated along the <110> direction. The outward oxygen movements are shown. Small and large black balls represent oxygen and titanium atoms, respectively, while gray balls describe lead atoms.

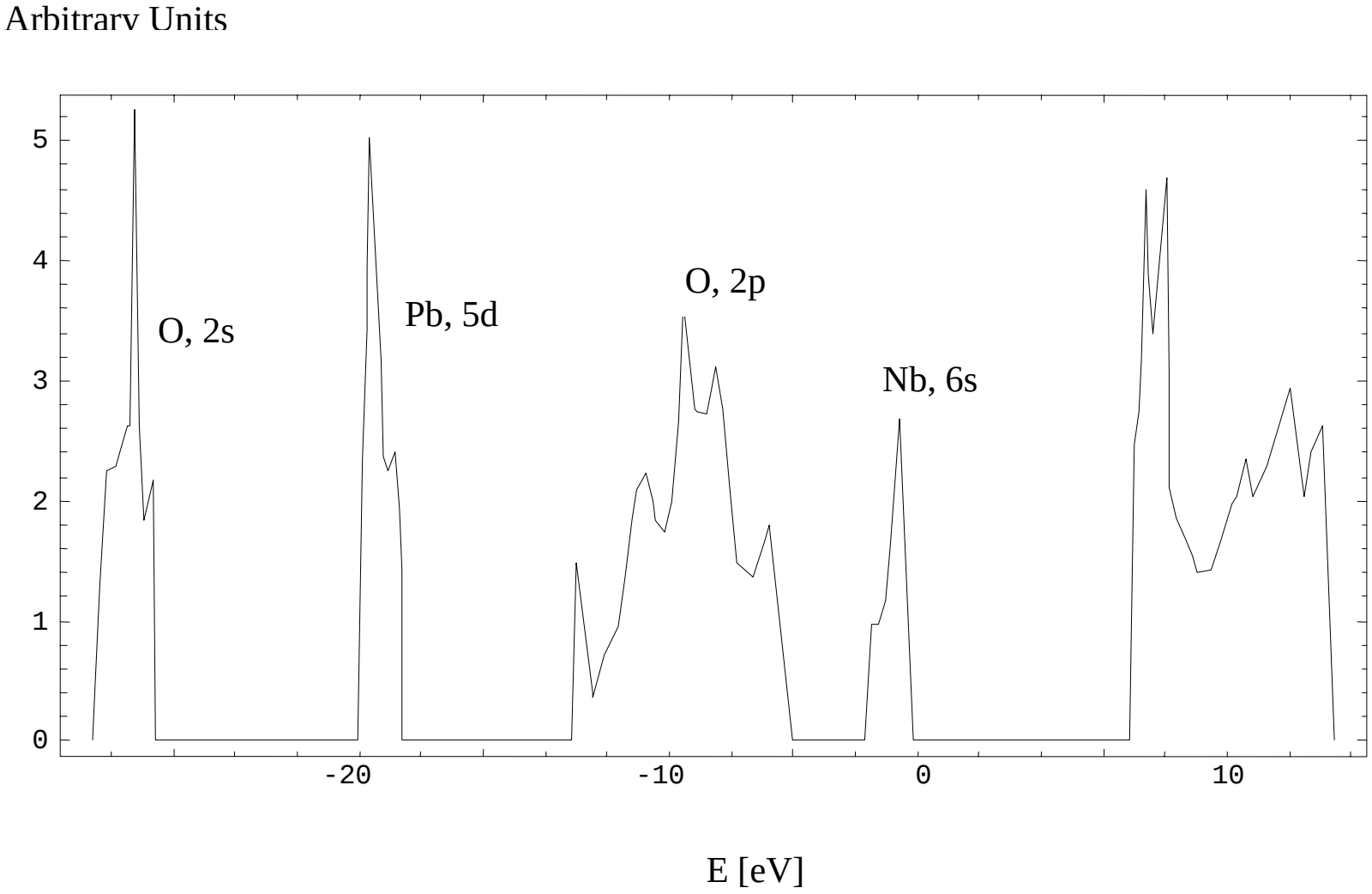
Arbitrary Units
5
4
3
2
1
0
-20
-10
0
10
O, 2s
Pb, 5d
O, 2p
Nb, 6s
E [eV]

Arbitrary Units

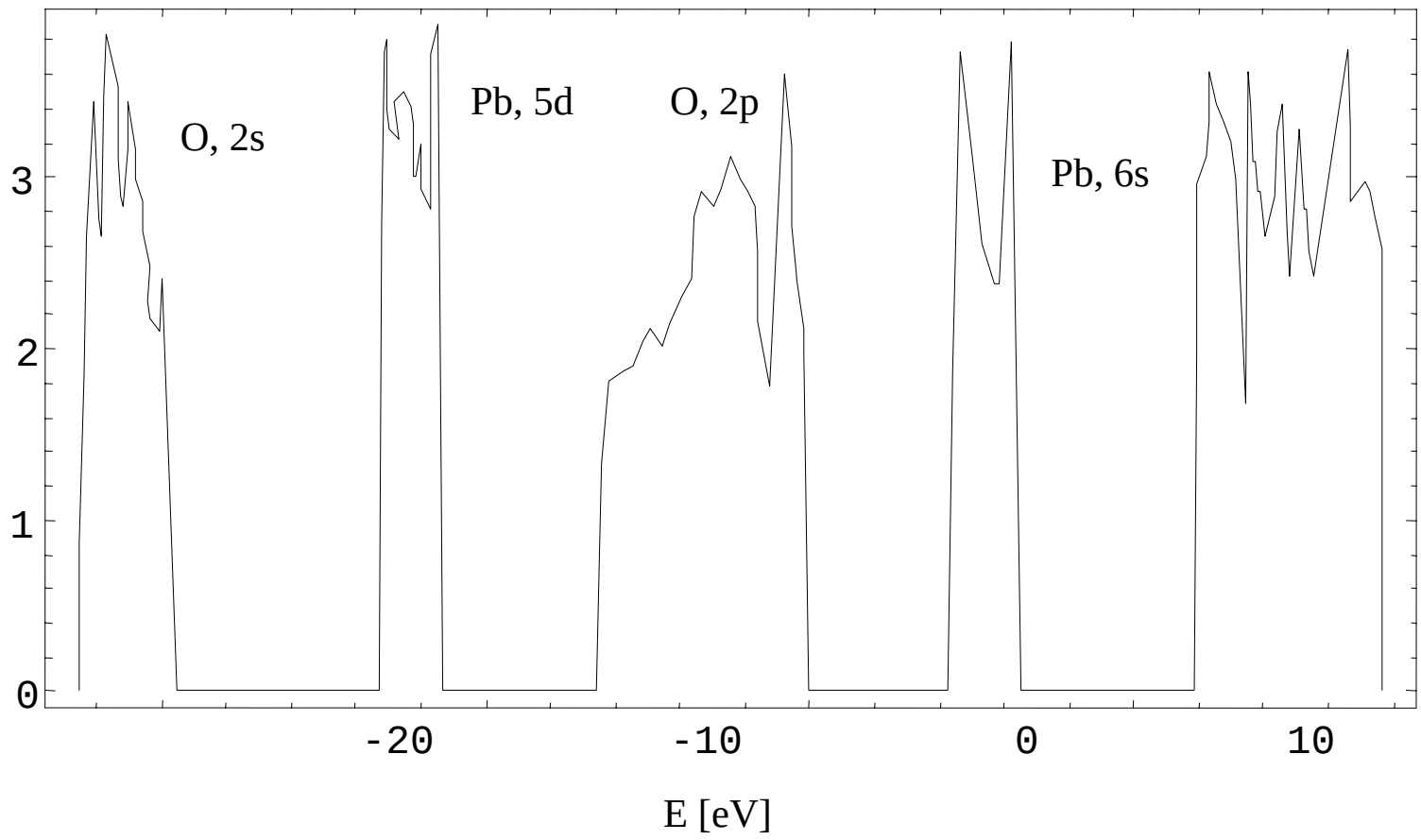

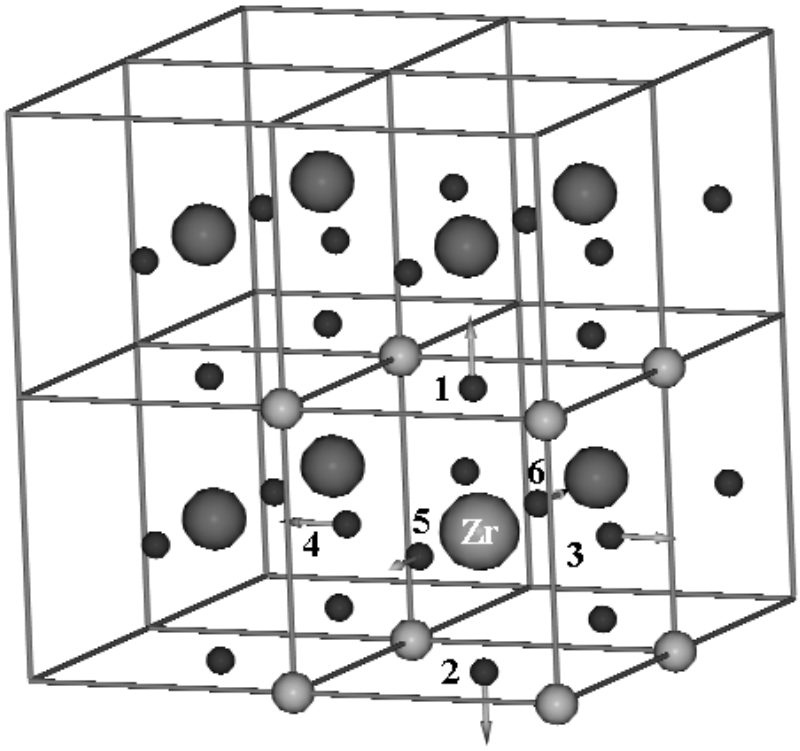
1
2
3
4
5
6
Zr

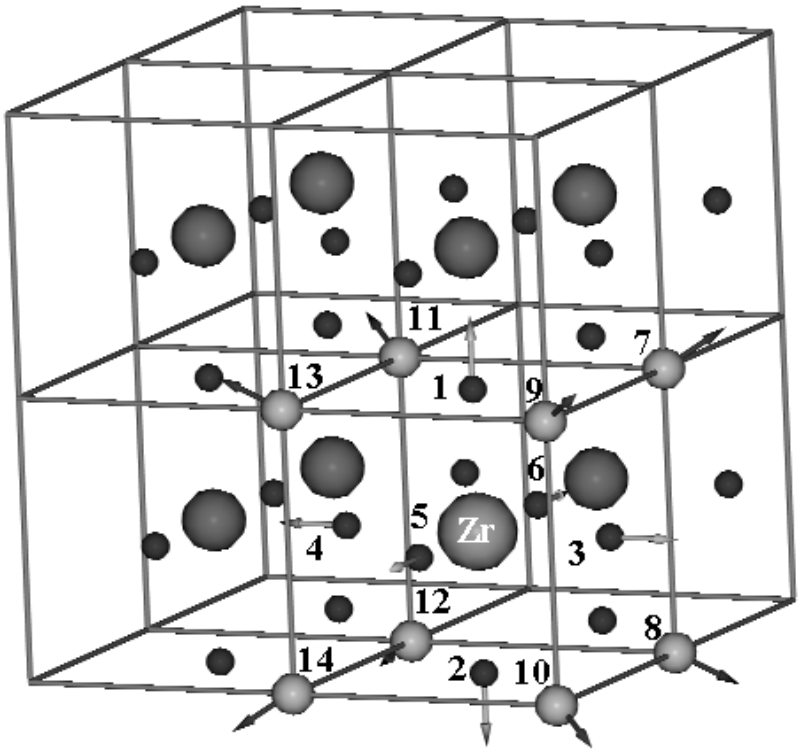
11
7
13
1
9
6
5
Zr
4
3
12
8
14
2
10

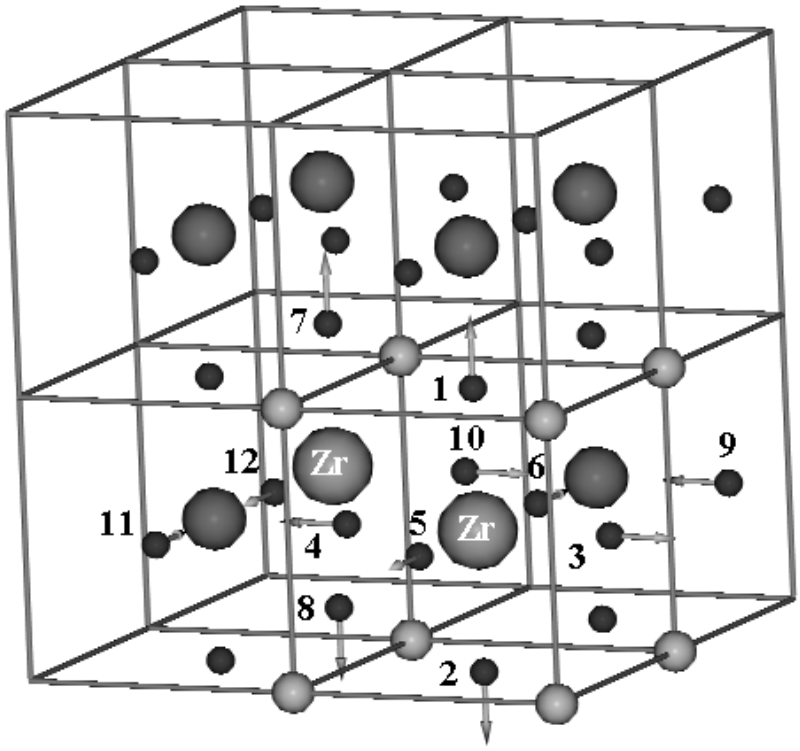
7
1
12
Zr
10
6
9
11
4
5
Zr
3
8
2